A TIME-FRACTIONAL MEAN-FIELD CONTROL MODELING SUBDIFFUSIVE ADVECTIVE TRANSPORT*

XIANGCHENG ZHENG†||, ZHIWEI YANG‡||, WUCHEN LI§, AND HONG WANG¶

Abstract. A time-fractional mean-field control (MFC) is developed for a prototype model of accidental spill of a hazardous contaminant in subsurface porous media, which is a representative and recurrent environmental threat to the public, to optimize the flow pattern so that the spilled contaminant is remediated with the minimal cost required to ensure the clean water supply. A strongly coupled nonlinear system of a multiple time-scale time-fractional transport equation and a backward multiple time-scale time-fractional Hamilton-Jacobi equation is derived using the first-order optimality condition. A sequentially decoupled time-stepping finite element method is derived for the numerical simulation of the MFC. Numerical experiments are presented to investigate the performance of the MFC, which show that the MFC determines an optimal flow pattern to ensure clean groundwater supply during and beyond the time period of contaminant spill with minimal cost.

Key words. mean field control, time-fractional, subdiffusive advective transport, Hamilton–Jacobi equation, decoupling algorithm

MSC codes. 35Q89, 35R11, 91A16

DOI. 10.1137/22M1527726

1. Introduction. Mean-field controls (MFCs) model dynamical behaviors of populations (e.g., particles/agents in physics/social systems), which have vast applications in robotics path planning, pandemic control, data science, conservation laws, reaction-diffusion equations, and finance [12, 23, 25, 26, 27, 29, 30, 32, 33, 36, 44, 55]. The minimizer system of MFCs leads to a pair of partial differential equations (PDEs) describing the optimal trajectory of the population dynamic.

The cost functional in most MFC research in the literature is constrained by (integer-order) PDEs [25, 29]. In recent years time-fractional MFCs were developed via stochastic analysis [7, 9, 50], and their well-posedness and regularity as well as numerical approximations were carried out rigorously [8, 10, 16]. Motivated by the successful developments and applications of the powerful MFCs, in this paper we develop a multiple time-scale time-fractional MFC to describe a prototype modeling of accidental spill of a hazardous contaminant in subsurface porous media, which is a representative and recurrent environmental threat to the public. The goal is to optimize the flow pattern so that the spilled contaminant is transported and remediated

^{*}Submitted to the journal's Computational Methods in Science and Engineering section October 10, 2022; accepted for publication (in revised form) August 31, 2023; published electronically December 7, 2023.

https://doi.org/10.1137/22M1527726

Funding: This work was partially funded by the Taishan Scholars Program of Shandong Province tsqn202306083, by the National Natural Science Foundation of China under grant 12301555, by the National Science Foundation under grant DMS-2012291, and by the China Postdoctoral Science Foundation under grants 2022M720809 and 2023T160109.

[†]School of Mathematics, Shandong University, Jinan 250100, China (xzheng@sdu.edu.cn).

[†]Research Institute of Intelligent Complex Systems, School of Mathematical Sciences, Fudan University, Shanghai 200433, China (zhiweiyang@fudan.edu.cn).

[§]Department of Mathematics, University of South Carolina, Columbia, SC 29208 USA (wuchen@mailbox.sc.edu).

[¶]Corresponding author. Department of Mathematics, University of South Carolina, Columbia, SC 29208 USA (hwang@math.sc.edu).

These authors contributed equally to this work and should be considered as co-first authors.

with the minimal cost required to ensure the clean water supply to the public during the entire time period of the spill and beyond.

In section 2 we recall that the time-fractional transport PDE provides more accurate description of the subdiffusive advective transport of contaminant through heterogeneous porous media than its integer-order counterpart does, which motivates the choice of the time-fractional transport PDE as the constraining equation for the MFC. Note that in the accidental spill of contaminant in subsurface formation, the transport process is not affected significantly by individual particles of the contaminant but will be determined by the aggregate behavior of particles, e.g., the concentration of the solute and the velocity field of the fluid. These observations suggest the use of the MFC (2.1), constrained by the time-fractional transport PDE (2.3) in order to accurately describe subdiffusive advective transport of the spilled contaminant through heterogeneous media.

In section 3 we address the solution procedure for the (time-fractional) MFC (2.1) and (2.3), to which there are two general approaches in the literature: One minimizes the MFC (2.1) and (2.3) directly via, e.g., primal-dual hybrid gradient methods [13, 30, 32], while the other utilizes the first-order optimality condition to derive a system of PDEs as the stationary point of the MFC formulation. In this paper we adopt the second approach by introducing a pseudopotential as a Lagrangian multiplier and applying the first-order optimality condition to derive a strongly coupled nonlinear system (3.8) of a multiple time-scale time-fractional subdiffusive advective transport PDE in terms of the concentration of the contaminant and a backward-intime multiple time-scale time-fractional Hamilton-Jacobi-Bellman PDE in terms of the pseudopotential that governs the velocity field.

In section 4 we develop a sequentially decoupled time-stepping finite element method to numerically simulate the coupled fractional PDE system (3.8) to obtain its numerical solution. In section 5 we carry out numerical experiments to investigate the performance of the MFC formulation: (i) We test the convergence of the numerical model. (ii) With the numerically justified convergence we conduct numerical experiments to examine the performance of the MFC in the context of control and elimination of contaminant in groundwater supply zones after an accidental leakage or spill of contaminant. Finally, section 6 contains concluding remarks. We summarize the results and observations of the paper and outline possible future research directions and obstacles in the context of subsurface flow and transport.

2. A multiple time-scale time-fractional MFC. Let $\Omega \subset \mathbb{R}^d$ with $1 \leq d \leq 3$ be a bounded aquifer with the boundary $\partial \Omega$. Consider a representative scenario: A hazardous contaminant is accidentally spilled in the subdomain $\Omega_s \subset \Omega$, the goal is to optimize the velocity field \boldsymbol{v} so that the contaminant is transported and remediated with the minimal transportation cost, and the contaminant is eliminated in the groundwater supply zone $\Omega_w \subset \Omega$ during the time period [0,T] and beyond. Then an MFC is formulated as follows [6,21]: Find the concentration $\rho:[0,T] \to L^2_+(\Omega)$ and the velocity field $\boldsymbol{v}:[0,T] \to H_0(\operatorname{div};\Omega)$ to minimize the cost functional

(2.1)
$$\inf_{\rho, \boldsymbol{v}, \rho_T} \int_0^T \int_{\Omega} \frac{1}{2} \rho(\boldsymbol{x}, t) |\boldsymbol{v}(\boldsymbol{x}, t)|^2 d\boldsymbol{x} dt + \int_{\Omega} G(\boldsymbol{x}, \rho_T(\boldsymbol{x})) d\boldsymbol{x}.$$

Here $L^2(\Omega)$ is the space of square integrable functions on Ω , $L^2_+(\Omega) := \{q \in L^2(\Omega) : q \geq 0\}$, $H_0(\operatorname{div};\Omega) := \{\boldsymbol{u} \in (L^2(\Omega))^d : \nabla \cdot \boldsymbol{u} \in L^2(\Omega), \ \boldsymbol{u} \cdot \boldsymbol{n} = 0 \text{ on } \partial\Omega\}$ with \boldsymbol{n} being the unit outward normal to $\partial\Omega$ and ∇ being the gradient operator, $\rho_T(\boldsymbol{x}) := \rho(\boldsymbol{x},T)$ is the terminal value, and the function G is convex with respect to ρ_T .

Remark 2.1. The first term accounts for the total kinetic energy required to transport the contaminant during the time period [0,T]. The second term may reduce to the weighted L^p norm with $p \geq 1$ for a properly chosen G that is supported on the water supply zone $\Omega_w \subset \Omega$ (cf. section 5). The MFC (2.1) and (2.3) ensures that the subdiffusive advective transport of the contaminant through the heterogeneous aquifer Ω governed by the time-fractional transport PDE (2.3) with the optimal velocity field v minimizes (i.e., cleans up) the contaminant in the water supply zone Ω_w with the minimal accumulated kinetic energy (to transport the contaminant to the right location to be remediated).

Recall that the integer-order Fickian diffusive advective transport PDE was derived under the assumptions that the underlying particle jumps have (i) a mean free path, and (ii) a mean waiting time [38], which are valid for transport in homogeneous media when solute plumes are observed to be Gaussian [4, 37, 38]. This justifies why the PDE, which admits Gaussian fundamental solutions, can accurately describe contaminant transport in homogeneous media. When extended to model transport in heterogeneous media by adjusting the variable parameters that multiply the preset integer-order differential operators to fit the training data, these PDEs tend to yield less accurate predictions [5, 11, 14, 19, 37, 38]. The reason is that transport in heterogeneous media exhibits highly skewed power-law decaying tails, which can hardly be captured by integer-order diffusive advective transport PDEs, characterized by a combination of Gaussian fundamental solutions, over a wide parameter range [5, 11, 14, 19, 37, 38].

Under the assumption that the mean waiting time has a power-law decaying tail as observed in field tests, the time-fractional diffusion PDE

$$(2.2) \qquad \qquad \partial_t^{\alpha} \rho - \Delta \rho = 0, \quad 0 < \alpha < 1, \quad \partial_t^{\alpha} g := \frac{1}{\Gamma(1 - \alpha)} \int_0^t \frac{g'(s) ds}{(t - s)^{\alpha}},$$

where ∂_t^{α} represents the fractional derivative operator with $\Gamma(\cdot)$ being the Gamma function [43] and Δ is the Laplacian, was derived via continuous time random walk (CTRW) and was shown to accurately describe transport in heterogeneous aquifers [37, 38, 46, 47]. However, (2.2) admits solutions with singularity near the initial time t=0, which is not physically relevant [45, 48], because (2.2) was derived as the diffusion limit of a CTRW in the phase plane and so holds only for large time t>0. This is why it fails to catch the Fickian diffusive behavior near the initial time t=0 [62], which will cause further complications to system (3.8) in the current context. The two time-scale mobile-immobile time-fractional PDE with the partition coefficient κ [46, 61],

$$\partial_t \rho + \kappa \partial_t^{\alpha} \rho - \Delta \rho = 0$$
, $\kappa > 0$, $0 < \alpha < 1$,

in which a $1/(1+\kappa)$ portion of the contaminant stays in the mobile phase and undergoes Fickian diffusive transport, while the rest gets absorbed to the aquifer and undergoes subdiffusive transport [14, 39, 64], accurately describes Fickian diffusive transport near the initial time and subdiffusive transport subsequently [46, 62].

We complete the MFC (2.1) by the two time-scale time-fractional PDE

(2.3)
$$\partial_{t}\rho + \kappa \partial_{t}^{\alpha}\rho - K\Delta\rho + \nabla \cdot (\rho \boldsymbol{v}(\boldsymbol{x}, t)) = f(\boldsymbol{x}, \bar{\rho}) \quad \text{in } \Omega \times (0, T],$$
$$\rho(\boldsymbol{x}, 0) = \rho_{0}(\boldsymbol{x}) \quad \text{on } \Omega,$$
$$\boldsymbol{v}(\boldsymbol{x}, t) \cdot \boldsymbol{n}(\boldsymbol{x}) = \nabla \rho(\boldsymbol{x}, t) \cdot \boldsymbol{n}(\boldsymbol{x}) = 0 \quad \text{on } \partial\Omega \times [0, T].$$

Here K > 0 is the diffusivity coefficient, $\rho_0 \in L^2_+(\Omega)$ refers to the initial value, $f(\boldsymbol{x}, \bar{\rho}) > 0$ with $\bar{\rho}$ being the prescribed concentration of the contaminant at sources, f < 0 with $\bar{\rho} = \rho$ being the concentration of the contaminant in the groundwater at sinks, and $f \equiv 0$ elsewhere.

3. A time-fractional PDE system from the optimality condition. We are now in the position to address the minimization of the MFC (2.1) and (2.3), for which there are two general approaches to finding the minimizers. The first is to minimize the MFC (2.1) and (2.3) directly via, e.g., primal-dual hybrid gradient methods [13, 30, 32], while the other is to utilize the first-order optimality condition to derive a system of PDEs as the stationary point of the optimization problem (2.1) and (2.3). In this paper we adopt the second approach.

To facilitate the derivation, introduce the specific momentum

(3.1)
$$\boldsymbol{m}(\boldsymbol{x},t) := \rho(\boldsymbol{x},t)\boldsymbol{v}(\boldsymbol{x},t).$$

Then the MFC (2.1) and (2.3) can be reformulated as

(3.2)
$$\inf_{\rho, \boldsymbol{m}, \rho_T} \int_0^T \int_{\Omega} \frac{|\boldsymbol{m}(\boldsymbol{x}, t)|^2}{2\rho(\boldsymbol{x}, t)} d\boldsymbol{x} dt + \int_{\Omega} G(\boldsymbol{x}, \rho_T(\boldsymbol{x})) d\boldsymbol{x},$$

which is subject to the constraint

(3.3)
$$\begin{aligned} \partial_t \rho + \kappa \partial_t^{\alpha} \rho - K \Delta \rho + \nabla \cdot \boldsymbol{m} &= f(\boldsymbol{x}, \bar{\rho}) & \text{in } \Omega \times (0, T], \\ \rho(\boldsymbol{x}, 0) &= \rho_0(\boldsymbol{x}) & \text{on } \Omega, \\ \boldsymbol{m}(\boldsymbol{x}, t) \cdot \boldsymbol{n}(\boldsymbol{x}) &= \nabla \rho(\boldsymbol{x}, t) \cdot \boldsymbol{n}(\boldsymbol{x}) &= 0 & \text{on } \partial \Omega \times [0, T]. \end{aligned}$$

Note from (3.1) that

$$\lim_{\rho \to 0^+} \frac{|\boldsymbol{m}|^2}{\rho} = 0,$$

and hence the specific kinetic energy term in (3.2) vanishes whenever $\rho(\boldsymbol{x},t) = 0$. Accordingly, if $\rho(\boldsymbol{x},t) = 0$ for $\boldsymbol{x} \in \partial \Omega$, we enforce $\boldsymbol{m}(\boldsymbol{x},t) \cdot \boldsymbol{n}(\boldsymbol{x}) = 0$.

Let $\phi(\boldsymbol{x},t)$ be a Lagrangian multiplier that is subject to the no-flux boundary condition

(3.5)
$$\nabla \phi(\mathbf{x}, t) \cdot \mathbf{n}(\mathbf{x}) = 0 \quad \text{on } \partial \Omega \times [0, T],$$

and let the cost functional be defined by

(3.6)
$$L(\rho, \boldsymbol{m}, \rho_T, \phi) := \int_0^T \int_{\Omega} \frac{|\boldsymbol{m}|^2}{2\rho} d\boldsymbol{x} dt + \int_{\Omega} G(\boldsymbol{x}, \rho_T) d\boldsymbol{x} - \int_0^T \int_{\Omega} \phi \left(\partial_t \rho + \kappa \partial_t^{\alpha} \rho - K \Delta \rho + \nabla \cdot \boldsymbol{m} - f(\boldsymbol{x}, \bar{\rho})\right) d\boldsymbol{x} dt.$$

Apply the Karush–Kuhn–Tucker approach to reformulate the constrained optimization problem (3.2)–(3.3) as an unconstrained optimization: Find a quadruple ρ , m, ρ_T , and ϕ to optimize the problem

(3.7)
$$\inf_{\rho, \boldsymbol{m}, \rho_T} \sup_{\phi} L(\rho, \boldsymbol{m}, \rho_T, \phi).$$

We utilize the optimality condition of problem (3.6)–(3.7) to compute the first variation of the generalized Lagrangian $L(\rho, \boldsymbol{m}, \rho_T, \phi)$ with respect to all its arguments to prove the following theorem.

Theorem 3.1. The optimization problem (3.6)–(3.7) can be characterized by the following coupled nonlinear time-fractional PDE system, which consists of a forward time-fractional PDE describing subdiffusive advective transport of the contaminant and a backward time-fractional Hamilton–Jacobi PDE describing the subdiffusive advective transport of the pseudopotential ϕ as the Lagrangian multiplier:

(3.8)
$$\partial_t \rho + \kappa \partial_t^{\alpha} \rho - K \Delta \rho - \nabla \cdot (\rho \nabla \phi) = f \qquad \text{in } \Omega \times (0, T],$$

$$\partial_t \phi - \kappa \hat{\partial}_t^{\alpha} \phi + K \Delta \phi - \frac{|\nabla \phi|^2}{2} + (\partial_{\rho} f) \phi = 0 \quad \text{in } \Omega \times [0, T),$$

$$\rho(\boldsymbol{x}, 0) = \rho_0(\boldsymbol{x}), \ \phi(\boldsymbol{x}, T) = \partial_{\rho_T} G(\boldsymbol{x}, \rho_T) \qquad \text{on } \Omega,$$

$$\nabla \rho(\boldsymbol{x}, t) \cdot \boldsymbol{n}(\boldsymbol{x}) = \nabla \phi(\boldsymbol{x}, t) \cdot \boldsymbol{n}(\boldsymbol{x}) = 0 \qquad \text{on } \partial\Omega \times [0, T].$$

Here the backward Riemann-Liouville fractional integral operator $_t\hat{I}_T^{1-\alpha}$ and differential operator $\hat{\partial}_t^{\alpha}$ are defined by [43]

$$(3.9) \qquad \qquad \hat{\partial}_t^{\alpha}g := -\partial_t \left({}_t \hat{I}_T^{1-\alpha}g \right), \quad {}_t \hat{I}_T^{1-\alpha} := \frac{1}{\Gamma(1-\alpha)} \int_t^T \frac{g(s)ds}{(s-t)^{\alpha}}.$$

Proof. Letting $\delta \phi$ be an admissible function that is subject to the boundary condition (3.5), we use (3.6) to compute the variation $\delta_{\phi}L(\rho, \boldsymbol{m}, \rho_T, \phi)$ with respect to following ϕ :

$$\begin{split} J_{\phi}(\theta) &:= L(\rho, \boldsymbol{m}, \rho_T, \phi + \theta \delta \phi) \\ &= \int_0^T \int_{\Omega} \frac{|\boldsymbol{m}|^2}{2\rho} d\boldsymbol{x} dt + \int_{\Omega} G(\boldsymbol{x}, \rho_T) d\boldsymbol{x} \\ &- \int_0^T \int_{\Omega} (\phi + \theta \delta \phi) \big(\partial_t \rho + \kappa \partial_t^{\alpha} \rho - K \Delta \rho + \nabla \cdot \boldsymbol{m} - f(\boldsymbol{x}, \bar{\rho}) \big) d\boldsymbol{x} dt. \end{split}$$

Differentiate $J_{\phi}(\theta)$ with respect to θ and then set $\theta = 0$ to obtain

$$\begin{split} &\delta_{\phi}L(\rho,\boldsymbol{m},\rho_{T},\phi) = J_{\phi}'(0) \\ &= -\int_{0}^{T}\int_{\Omega}\delta\phi\big(\partial_{t}\rho + \kappa\partial_{t}^{\alpha}\rho - K\Delta\rho + \nabla\cdot\boldsymbol{m} - f(\boldsymbol{x},\bar{\rho})\big)d\boldsymbol{x}dt = 0. \end{split}$$

Since $\delta \phi$ is arbitrary, we obtain the following time-fractional PDE for the concentration ρ :

$$(3.10) \quad \partial_t \rho(\mathbf{x}, t) + \kappa \partial_t^{\alpha} \rho(\mathbf{x}, t) - K \Delta \rho(\mathbf{x}, t) + \nabla \cdot \mathbf{m}(\mathbf{x}, t) = f(\mathbf{x}, \bar{\rho}) \quad \text{in } \Omega \times (0, T].$$

To compute the variation $\delta_{\rho}L(\rho, \boldsymbol{m}, \rho_T, \phi)$ with respect to ρ , we use the forward differential operator ∂_t^{α} in (2.2) and the backward differential operator $\hat{\partial}_t^{\alpha}$ in (3.9) to integrate the $\phi \partial_t^{\alpha} \rho$ term in the last integral on the right-hand side of (3.6) to find

$$\int_{\Omega} \int_{0}^{T} \phi(\boldsymbol{x},t) \, \partial_{t}^{\alpha} \rho(\boldsymbol{x},t) dt d\boldsymbol{x} \\
= \frac{1}{\Gamma(1-\alpha)} \int_{\Omega} \left[\int_{0}^{T} \phi(\boldsymbol{x},t) \int_{0}^{t} \frac{\partial_{s} \rho(\boldsymbol{x},s) ds}{(t-s)^{\alpha}} dt \right] d\boldsymbol{x} \\
= \frac{1}{\Gamma(1-\alpha)} \int_{\Omega} \int_{0}^{T} \left[\int_{0}^{t} \frac{\phi(\boldsymbol{x},t) \partial_{s} \rho(\boldsymbol{x},s)}{(t-s)^{\alpha}} ds \right] dt d\boldsymbol{x} \\
= \frac{1}{\Gamma(1-\alpha)} \int_{\Omega} \int_{0}^{T} \left[\int_{s}^{T} \frac{\phi(\boldsymbol{x},t) \partial_{s} \rho(\boldsymbol{x},s)}{(t-s)^{\alpha}} dt \right] ds d\boldsymbol{x} \\
= \int_{\Omega} \int_{0}^{T} \left[\partial_{s} \rho(\boldsymbol{x},s) \frac{1}{\Gamma(1-\alpha)} \int_{s}^{T} \frac{\phi(\boldsymbol{x},t)}{(t-s)^{\alpha}} dt \right] ds d\boldsymbol{x} \\
= \int_{\Omega} \int_{0}^{T} \rho(\boldsymbol{x},s) \hat{\partial}_{s}^{\alpha} \phi(\boldsymbol{x},s) ds d\boldsymbol{x} - \int_{\Omega} \rho_{0}(\boldsymbol{x})_{0} \hat{I}_{T}^{1-\alpha} \phi(\boldsymbol{x},s) d\boldsymbol{x}.$$

Integrate the remaining terms in the last integral of (3.6) by parts and use (3.11) and the space-time boundary conditions in (3.3) to find

(3.12)
$$\int_{0}^{T} \int_{\Omega} \phi \left(\partial_{t} \rho + \kappa \partial_{t}^{\alpha} \rho - K \Delta \rho + \nabla \cdot \boldsymbol{m} - f(\boldsymbol{x}, \bar{\rho}) \right) d\boldsymbol{x} dt$$

$$= \int_{0}^{T} \int_{\Omega} \rho \left(-\partial_{t} \phi + \kappa \hat{\partial}_{t}^{\alpha} \phi - K \Delta \phi \right) - \boldsymbol{m} \cdot \nabla \phi - \phi f(\boldsymbol{x}, \bar{\rho}) d\boldsymbol{x} dt$$

$$+ \int_{\Omega} \rho_{T}(\boldsymbol{x}) \phi(\boldsymbol{x}, T) d\boldsymbol{x} - \int_{\Omega} \rho_{0}(\boldsymbol{x}) \left[\phi(\boldsymbol{x}, 0) + \kappa_{0} \hat{I}_{T}^{1-\alpha} \phi(\boldsymbol{x}, \cdot) \right] d\boldsymbol{x}.$$

Let $\delta \rho$ be any admissible function satisfying the homogeneous boundary, initial, and terminal conditions

(3.13)
$$\delta \rho(\boldsymbol{x},0) = \delta \rho(\boldsymbol{x},T) = 0 \text{ on } \Omega, \quad \nabla \delta \rho(\boldsymbol{x},t) \cdot \boldsymbol{n}(\boldsymbol{x}) = 0 \text{ on } \partial \Omega \times [0,T].$$

Combine (3.6) and (3.12) and utilize (3.13) to obtain

$$\begin{split} J_{\rho}(\theta) &:= L(\rho + \theta \delta \rho, \boldsymbol{m}, \rho_{T}, \phi) \\ &= \int_{0}^{T} \int_{\Omega} \frac{|\boldsymbol{m}|^{2}}{2(\rho + \theta \delta \rho)} d\boldsymbol{x} dt + \int_{\Omega} G(\boldsymbol{x}, \rho_{T}) d\boldsymbol{x} dt \\ &- \int_{0}^{T} \int_{\Omega} \phi \left(\partial_{t} \rho + \kappa \partial_{t}^{\alpha} \rho - K \Delta \rho + \nabla \cdot \boldsymbol{m} - f(\boldsymbol{x}, \bar{\rho}) \right) \Big|_{\rho = \rho + \theta \delta \rho} d\boldsymbol{x} dt \\ &= \int_{0}^{T} \int_{\Omega} \frac{|\boldsymbol{m}|^{2}}{2(\rho + \theta \delta \rho)} d\boldsymbol{x} dt + \int_{\Omega} G(\boldsymbol{x}, \rho_{T}) d\boldsymbol{x} dt \\ &- \int_{0}^{T} \int_{\Omega} \left[(\rho + \theta \delta \rho) \left(- \partial_{t} \phi + \kappa \hat{\partial}_{t}^{\alpha} \phi - K \Delta \phi \right) - \boldsymbol{m} \cdot \nabla \phi \right] \\ &- \phi(\boldsymbol{x}, t) f(\boldsymbol{x}, \bar{\rho}) \Big|_{\rho = \rho + \theta \delta \rho} d\boldsymbol{x} dt - \int_{\Omega} \rho_{T}(\boldsymbol{x}) \phi(\boldsymbol{x}, T) d\boldsymbol{x} \\ &+ \int_{\Omega} \rho_{0}(\boldsymbol{x}) \left[\phi(\boldsymbol{x}, 0) + \kappa_{0} \hat{I}_{T}^{1 - \alpha} \phi(\boldsymbol{x}, \cdot) \right] d\boldsymbol{x}. \end{split}$$

Differentiating $J_{\rho}(\theta)$ with respect to θ yields

$$\begin{split} J_{\rho}'(\theta) &= \int_{0}^{T} \int_{\Omega} -\frac{|\boldsymbol{m}|^{2} \delta \rho}{2(\rho + \theta \delta \rho)^{2}} d\boldsymbol{x} dt \\ &- \int_{0}^{T} \int_{\Omega} \delta \rho \Big(-\partial_{t} \phi + \kappa \hat{\partial}_{t}^{\alpha} \phi - K \Delta \phi - \phi \partial_{\rho} f(\boldsymbol{x}, \bar{\rho}) \Big|_{\rho = \rho + \theta \delta \rho} \Big) d\boldsymbol{x} dt. \end{split}$$

Then set $\theta = 0$ gives rise to

$$\begin{split} \delta_{\rho}L(\rho,\boldsymbol{m},\rho_{T},\phi) &= J_{\rho}'(0) \\ &= \int_{0}^{T} \int_{\Omega} \delta\rho \bigg[\partial_{t}\phi - \kappa \hat{\partial}_{t}^{\alpha}\phi + K\Delta\phi + \phi \partial_{\rho}f - \frac{|\boldsymbol{m}|^{2}}{2\rho^{2}} \bigg] d\boldsymbol{x} dt = 0. \end{split}$$

The arbitrary $\delta \rho$ yields the backward time-fractional Hamilton–Jacobi PDE for ϕ :

(3.14)
$$\partial_t \phi - \kappa \hat{\partial}_t^{\alpha} \phi + K \Delta \phi + (\partial_{\rho} f) \phi - \frac{|\boldsymbol{m}|^2}{2\rho^2} = 0 \text{ in } \Omega \times [0, T].$$

Similarly, let δm be any admissible function satisfying the no-flow boundary condition in (3.3). Use (3.6), (3.12), and the boundary condition (3.3) for δm to deduce

$$egin{aligned} J_{m{m}}(heta) &:= L(
ho, m{m} + heta \delta m{m},
ho_T, \phi) \ &= \int_0^T \int_\Omega rac{|m{m} + heta \delta m{m}|^2}{2
ho} dm{x} dt + \int_\Omega G(m{x},
ho_T) dm{x} \ &- \int_0^T \int_\Omega \phi ig(\partial_t
ho + \kappa \partial_t^lpha
ho - K \Delta
ho - f(m{x}, ar{
ho})ig) - (m{m} + heta \delta m{m}) \cdot
abla \phi dm{x} dt. \end{aligned}$$

Differentiate $J_{\boldsymbol{m}}(\theta)$ with respect to θ and then set $\theta = 0$ to obtain

(3.15)
$$\delta_{\boldsymbol{m}} L(\rho, \boldsymbol{m}, \rho_T, \phi) = J'_{\boldsymbol{m}}(0) = \int_0^T \int_{\Omega} \frac{\boldsymbol{m} \cdot \delta \boldsymbol{m}}{\rho} + \delta \boldsymbol{m} \cdot \nabla \phi d\boldsymbol{x} dt = 0.$$

Since δm is arbitrary, we use (3.1) and (3.15) to derive

$$\mathbf{v} = \frac{\mathbf{m}}{\rho} = -\nabla\phi.$$

Put $\mathbf{m} = \rho \mathbf{v} = -\rho \nabla \phi$ in (3.10) and (3.14) to obtain the two time-fractional PDEs for ρ and ϕ and the no-flux boundary condition for ϕ in (3.8).

Finally, let $\delta \rho_T$ be any admissible function. Use (3.6) and (3.12) to find

$$\begin{split} J_{\rho_T}(\theta) &:= L(\rho, \boldsymbol{m}, \rho_T + \theta \delta \rho_T, \phi) \\ &= \int_0^T \int_{\Omega} \frac{|\boldsymbol{m}|^2}{2\rho} d\boldsymbol{x} dt + \int_{\Omega} G(\boldsymbol{x}, \rho_T + \theta \delta \rho_T) d\boldsymbol{x} \\ &- \int_0^T \int_{\Omega} \rho \left(-\partial_t \phi + \kappa \hat{\partial}_s^{\alpha} \phi - K \Delta \phi \right) - \boldsymbol{m} \cdot \nabla \phi - \phi f(\boldsymbol{x}, \rho) d\boldsymbol{x} dt \\ &- \int_{\Omega} \left(\rho_T(\boldsymbol{x}) + \theta \delta \rho_T \right) \phi(\boldsymbol{x}, T) d\boldsymbol{x} + \int_{\Omega} \rho_0(\boldsymbol{x}) \left(\phi(\boldsymbol{x}, 0) + \kappa_0 \hat{I}_T^{1-\alpha} \phi(\boldsymbol{x}, \cdot) \right) d\boldsymbol{x}. \end{split}$$

Differentiate $J_{\rho_T}(\theta)$ with respect to θ and then set $\theta = 0$ to obtain

$$\delta_{\rho_T} L(\rho, \boldsymbol{m}, \rho_T, \phi) = J'_{\rho_T}(0) = \int_{\Omega} \delta \rho_T (\partial_{\rho_T} G - \phi(\boldsymbol{x}, T)) d\boldsymbol{x} = 0.$$

We derive a terminal condition for ϕ at the final time t = T:

(3.17)
$$\phi(\boldsymbol{x},T) = \partial_{\rho_T} G(\boldsymbol{x},\rho_T).$$

We combine (3.17) with the initial conditions in (2.3) to obtain the initial condition for ρ and the terminal condition for ϕ in (3.8), thus proving the theorem.

- 4. A sequentially decoupled time-stepping finite element method. We take advantage of the physical properties of the subdiffusive advective flow and transport mechanism to develop a sequentially decoupled time-stepping finite element method for the numerical simulation of system (3.8) to optimize the flow pattern for the minimal transport cost.
- 4.1. A sequentially decoupling of system (3.8). The dependent variable of primary interest is the concentration ρ of the contaminant, which is solved from the forward time-fractional PDE in (3.8) that is determined by the velocity field $\mathbf{v} = -\nabla \phi$. This in turn relies on an accurate solution of ϕ in the backward time-fractional PDE in (3.8), which is coupled to the forward time-fractional PDE via $\partial_{\rho} f$ through ρ .

A sequentially decoupled backward Hamilton–Jacobi PDE. Define an initial guess for $\rho^{(0)}$ and $\rho_T^{(0)}$ by

$$\rho^{(0)}(\boldsymbol{x},t) := \rho_0(\boldsymbol{x}), \quad \rho_T^{(0)}(\boldsymbol{x}) := \rho_0(\boldsymbol{x}), \quad \boldsymbol{x} \in \Omega, \, t \in [0,T].$$

For m = 1, 2, ..., a sequentially decoupled terminal-boundary value problem of the backward time-fractional Hamilton–Jacobi PDE can be formulated for $\phi^{(m)}(\boldsymbol{x}, t)$:

$$(4.1) \begin{array}{l} \partial_{t}\phi^{(m)}(\boldsymbol{x},t) - \kappa \hat{\partial}_{t}^{\alpha}\phi^{(m)}(\boldsymbol{x},t) + K\Delta\phi^{(m)}(\boldsymbol{x},t) \\ -\frac{1}{2}|\nabla\phi^{(m)}(\boldsymbol{x},t)|^{2} + \partial_{\rho}f(\boldsymbol{x},\bar{\rho}^{(m-1)}(\boldsymbol{x},t))\phi^{(m)}(\boldsymbol{x},t) = 0 & \text{in } \Omega \times [0,T), \\ \phi^{(m)}(\boldsymbol{x},T) = \partial_{\rho_{T}}G(\boldsymbol{x},\rho_{T}^{(m-1)}(\boldsymbol{x})) & \text{on } \Omega, \\ \nabla\phi^{(m)}(\boldsymbol{x},t) \cdot \boldsymbol{n}(\boldsymbol{x}) = 0 & \text{on } \partial\Omega \times [0,T]. \end{array}$$

Let $H^1(\Omega)$ be the Sobolev space that consists of the Lebesgue square integrable functions on Ω with square integrable weak derivatives, equipped with the usual inner product and norm [21]. A backward weak formulation for problem (4.1) can be obtained by multiplying the fractional PDE in (4.1) by any test function $\chi \in H^1(\Omega)$, integrating the resulting equation on Ω , and applying the divergence theorem:

$$(\partial_{t}\phi^{(m)}(\cdot,t) - \kappa \hat{\partial}_{t}^{\alpha}\phi^{(m)}(\cdot,t), \chi) - (K\nabla\phi^{(m)}(\cdot,t), \nabla\chi) - (\frac{1}{2}|\nabla\phi^{(m)}(\cdot,t)|^{2}, \chi)$$

$$+ (\partial_{\rho}f(\cdot,\bar{\rho}^{(m-1)}(\cdot,t))\phi^{(m)}(\cdot,t), \chi) = 0, \quad 0 \le t < T,$$

$$(\phi^{(m)}(\cdot,T) - \partial_{\rho_{T}}G(\cdot,\rho_{T}^{(m-1)}(\cdot)), \chi) = 0,$$

with (\cdot, \cdot) representing the L_2 inner product over Ω .

A sequentially decoupled transport PDE. Given $\phi^{(m)}(\boldsymbol{x},t)$, solve for $\rho^{(m)}(\boldsymbol{x},t)$:

(4.3)
$$\begin{aligned} \partial_{t}\rho^{(m)}(\boldsymbol{x},t) + \kappa \partial_{t}^{\alpha}\rho^{(m)}(\boldsymbol{x},t) - \nabla \cdot \left(\rho^{(m)}(\boldsymbol{x},t)\nabla\phi^{(m)}(\boldsymbol{x},t)\right) \\ - K\Delta\rho^{(m)}(\boldsymbol{x},t) = f(\boldsymbol{x},\bar{\rho}^{(m)}(\boldsymbol{x},t)) & \text{in } \Omega \times (0,T], \\ \rho^{(m)}(\boldsymbol{x},0) = \rho_{0}(\boldsymbol{x}) & \text{on } \Omega, \\ \nabla\rho^{(m)}(\boldsymbol{x},t) \cdot \boldsymbol{n}(\boldsymbol{x}) = 0 & \text{on } \partial\Omega \times [0,T]. \end{aligned}$$

By the discussions following (3.4), $\bar{\rho}^{(m)} = \bar{\rho}$ at sources and $\bar{\rho}^{(m)} = \rho^{(m)}$ at sinks, and $f \equiv 0$ elsewhere. $\rho_T^{(m)}(\boldsymbol{x}) = \rho^{(m)}(\boldsymbol{x}, T)$. A forward weak formulation for problem (4.1) for any $\chi \in H^1(\Omega)$ is:

$$(\partial_{t}\rho^{(m)}(\cdot,t) + \kappa \partial_{t}^{\alpha}\rho^{(m)}(\cdot,t),\chi) + (K\nabla\rho^{(m)}(\cdot,t),\nabla\chi)$$

$$+ (\rho^{(m)}(\cdot,t)\nabla\phi^{(m)}(\cdot,t),\nabla\chi) = (f(\cdot,\bar{\rho}^{(m)}(\cdot,t)),\chi), \quad 0 < t \le T,$$

$$(\rho^{(m)}(\cdot,0) - \rho_{0}(\cdot),\chi) = 0.$$

4.2. A time-stepping finite element approximation to system (3.8).

Discretization of the sequentially decoupled time-fractional transport PDE (4.3). Define a temporal partition of [0,T] by

$$(4.5) 0 =: t_0 < t_1 < \dots < t_n < \dots < t_N := T, \tau_n := t_n - t_{n-1}, n = 1, 2, \dots, N.$$

Use the L1 discretization to approximate $\partial_t \rho^{(m)}(\boldsymbol{x}, t_n)$ and $\partial_t^{\alpha} \rho^{(m)}(\boldsymbol{x}, t_n)$ in the weak formulation (4.4) [34, 35, 49]. For $1 \leq n \leq N$

$$(4.6)$$

$$\partial_{t}\rho(\boldsymbol{x},t_{n}) \approx \delta_{\tau}\rho(\boldsymbol{x},t_{n}) := \frac{\rho(\boldsymbol{x},t_{n}) - \rho(\boldsymbol{x},t_{n-1})}{\tau_{n}},$$

$$\partial_{t}^{\alpha}\rho(\boldsymbol{x},t_{n}) = \sum_{k=1}^{n} \int_{t_{k-1}}^{t_{k}} \frac{\partial_{s}\rho(\boldsymbol{x},s)ds}{\Gamma(1-\alpha)(t_{n}-s)^{\alpha}} \approx \sum_{k=1}^{n} \int_{t_{k-1}}^{t_{k}} \frac{\delta_{\tau}\rho(\boldsymbol{x},t_{k})ds}{\Gamma(1-\alpha)(t_{n}-s)^{\alpha}}$$

$$= b_{n,n}\rho(\boldsymbol{x},t_{n}) + \sum_{k=1}^{n-1} (b_{n,k} - b_{n,k+1})\rho(\boldsymbol{x},t_{k}) - b_{n,1}\rho_{0}(\boldsymbol{x}) =: \delta_{\tau}^{\alpha}\rho(\boldsymbol{x},t_{n}),$$

$$b_{n,k} := \frac{(t_{n} - t_{k-1})^{1-\alpha} - (t_{n} - t_{k})^{1-\alpha}}{\Gamma(2-\alpha)\tau_{k}}, \quad 1 \leq k \leq n.$$

Let $S_h(\Omega) \subset H^1(\Omega)$ be a piecewise-linear finite element space with respect to a quasi-uniform partition of diameter h. Substituting $\delta_{\tau}\rho^{(m)}(\cdot,t_n)$ and $\delta_{\tau}^{\alpha}\rho^{(m)}(\cdot,t_n)$ for $\partial_t \rho^{(m)}(\cdot,t_n)$ and $\partial_t^{\alpha}\rho^{(m)}(\cdot,t_n)$ in (4.4) yields a time-stepping finite element scheme: For $n=1,2,\ldots,N$, find the finite element solution $\rho^{(m)}(\boldsymbol{x},t_n) \in S_h(\Omega)$ such that

$$(\delta_{\tau}\rho^{(m)}(\cdot,t_{n}) + \kappa\delta_{\tau}^{\alpha}\rho^{(m)}(\cdot,t_{n}),\chi) + (K\nabla\rho^{(m)}(\cdot,t_{n}),\nabla\chi)$$

$$+(\rho^{(m)}(\cdot,t_{n})\nabla\phi^{(m)}(\cdot,t_{n}),\nabla\chi) = (f(\cdot,\bar{\rho}^{(m)}(\cdot,t_{n})),\chi) \quad \forall \chi \in S_{h}(\Omega),$$

$$(\rho^{(m)}(\cdot,0) - \rho_{0}(\cdot),\chi) = 0 \quad \forall \chi \in S_{h}(\Omega).$$

Discretization of the sequentially decoupled backward time-fractional Hamilton–Jacobi PDE. Similarly discretize $\partial_t \phi^{(m)}(\boldsymbol{x},t)$ and $\hat{\partial}_t^{\alpha} \phi^{(m)}(\boldsymbol{x},t)$ backward in time on the partition (4.5) for $n = N, N - 1, \ldots, 1$:

$$\partial_{t}\phi(\mathbf{x},t_{n-1}) \approx \delta_{\tau}\phi(\mathbf{x},t_{n}),$$

$$\hat{\partial}_{t}^{\alpha}\phi(\mathbf{x},t_{n-1}) = -\partial_{t}\left(t_{n}\hat{I}_{T}^{1-\alpha}\phi\right)\Big|_{t=t_{n-1}} \approx -\frac{1}{\tau_{n}}\left[t_{n}\hat{I}_{T}^{1-\alpha}\phi - t_{n-1}\hat{I}_{T}^{1-\alpha}\phi\right]$$

$$= \frac{1}{\tau_{n}}\frac{1}{\Gamma(1-\alpha)}\left[\sum_{k=n}^{N}\int_{t_{k-1}}^{t_{k}}\frac{\phi(\mathbf{x},s)ds}{(s-t_{n-1})^{\alpha}} - \sum_{k=n}^{N-1}\int_{t_{k}}^{t_{k+1}}\frac{\phi(\mathbf{x},s)ds}{(s-t_{n})^{\alpha}}\right]$$

$$\approx \frac{1}{\tau_{n}}\frac{1}{\Gamma(1-\alpha)}\left[\sum_{k=n}^{N}\int_{t_{k-1}}^{t_{k}}\frac{\phi(\mathbf{x},t_{k-1})ds}{(s-t_{n-1})^{\alpha}} - \sum_{k=n}^{N-1}\int_{t_{k}}^{t_{k+1}}\frac{\phi(\mathbf{x},t_{k})ds}{(s-t_{n})^{\alpha}}\right]$$

$$= b_{n,n}\phi(\mathbf{x},t_{n-1}) + \sum_{k=n+1}^{N}(b_{k,n}-b_{k,n+1})\phi(\mathbf{x},t_{k-1}) =: \hat{\delta}_{\tau}^{\alpha}\phi(\mathbf{x},t_{n-1}),$$

$$b_{k,n} := \frac{(t_{k}-t_{n-1})^{1-\alpha}-(t_{k-1}-t_{n-1})^{1-\alpha}}{\Gamma(2-\alpha)\tau_{n}}, \quad n \leq k \leq N.$$

Here $\delta_{\tau_n}\phi(\boldsymbol{x},t_n)$ is defined in (4.6).

Substitute $\delta_{\tau}\phi^{(m)}(\cdot,t_n)$ and $\hat{\delta}_{\tau}^{\alpha}\phi^{(m)}(\cdot,t_{n-1})$ for $\partial_t\phi^{(m)}(\cdot,t_{n-1})$ and $\hat{\partial}_t^{\alpha}\phi^{(m)}(\cdot,t_{n-1})$ in (4.2), respectively, to derive a backward time-stepping finite element scheme: For $n=N,\ N-1,\ldots,1$, find the finite element solution $\phi^{(m)}(\boldsymbol{x},t_{n-1})\in S_h(\Omega)$ such that

$$(\delta_{\tau}\phi^{(m)}(\cdot,t_{n}) - \kappa\hat{\delta}_{\tau}^{\alpha}\phi^{(m)}(\cdot,t_{n-1}),\chi) - (K\nabla\phi^{(m)}(\cdot,t_{n-1}),\nabla\chi)$$

$$-\left(\frac{1}{2}|\nabla\phi^{(m)}(\cdot,t_{n-1})|^{2},\chi\right) + \left(\partial_{\rho}f(\cdot,\bar{\rho}^{(m-1)}(\cdot,t_{n-1}))\phi^{(m)}(\cdot,t_{n-1}),\chi\right) = 0,$$

$$(\phi^{(m)}(\cdot,T) - \partial_{\rho_{T}}G(\cdot,\rho_{T}^{(m-1)}(\cdot)),\chi) = 0 \quad \forall \chi \in S_{h}(\Omega).$$

Implementation. Let $\{\chi_i\}_{i=1}^{N_x} \subset S_h(\Omega)$ be the nodal basis and write $\phi(\cdot, t_{n-1})$ as

$$\phi(\boldsymbol{x},t_{n-1}) = \sum_{j=1}^{N_x} \phi_j \chi_j(\boldsymbol{x}), \quad \boldsymbol{x} \in \overline{\Omega}, \quad \phi_j := \phi(\boldsymbol{x}_j,t_{n-1}).$$

Evaluate the residual vector $\mathbf{r}(\phi) = [r_1(\phi), \dots, r_{N_x}(\phi)]^{\top}$,

$$\begin{split} r_i(\phi) &= \left(\delta_\tau \phi(\cdot, t_n) - \kappa \hat{\delta}_\tau^\alpha \phi(\cdot, t_{n-1}), \chi_i\right) - \left(K \nabla \phi(\cdot, t_{n-1}), \nabla \chi_i\right) \\ &- \left(\frac{1}{2} \left|\nabla \phi(\cdot, t_{n-1})\right|^2, \chi_i\right) + \left(\partial_\rho f(\cdot, \bar{\rho}(\cdot, t_{n-1})) \phi(\cdot, t_{n-1}), \chi_i\right), \end{split}$$

and the Jacobian matrix $\boldsymbol{J}(\phi) = [J_{i,j}(\phi)]_{i,j=1}^{N_x}$ by (4.8),

$$J_{i,j}(\phi) = -\frac{\partial r_i(\phi)}{\partial \phi_j} = \frac{1}{\tau_n} \left[1 + \frac{\kappa \tau_n^{1-\alpha}}{\Gamma(2-\alpha)} \right] (\chi_j, \chi_i) + (K \nabla \chi_j, \nabla \chi_i) + (\nabla \phi(\cdot, t_{n-1}) \cdot \nabla \chi_j, \chi_i) - (\partial_\rho f(\cdot, \bar{\rho}^{(m)}(\cdot, t_{n-1})) \chi_j, \chi_i).$$

By the discussions following (2.3), $-\partial_{\rho}f > 0$ at sinks and vanishes elsewhere. The last term is symmetric and positive semidefinite, and the first two terms are symmetric and positive definite. The third term may be indefinite. Hence, the Jacobi matrix J is nonsingular if τ_n is sufficiently small such that the Newton's method converges in the solution of the nonlinear system, as used in, e.g., optimal control of nonlinear evolution equations [28, 41, 51].

- 5. Numerical investigation. We conduct numerical experiments to test the convergence of the time-fractional MFC approximation (4.7) and (4.9). Then we examine the performance of the MFC to assess the effect of control and elimination of the contaminant in the groundwater supply zone in the context of a prototype modeling of accidental spill of a hazardous contaminant in one- and two-dimensional subsurface porous media.
- **5.1. Performance of the one-dimensional MFC.** The problem setting is as follows: The aquifer $\Omega = (0,1)$, the contaminant spill zone $\Omega_s = (0,0.1)$, the groundwater supply zone $\Omega_w = (0.9,1)$, and the diffusivity coefficient K = 0.001.
- **5.1.1. Numerical experiment 1(a).** In this set of numerical experiments, the source and sink term f is of the form

(5.1)
$$f(x,\bar{\rho}) = \begin{cases} \psi(x;0,0.1)\,\bar{\rho}, & x \in [0,0.5], \\ -\psi(x;0.9,1)\,\rho, & x \in [0.5,1], \end{cases}$$

where $\psi(x; z_1, z_2)$ is a mollified point source of the form

$$(5.2) \qquad \psi(x;z_1,z_2) := \operatorname{erf}\left(\frac{x-z_1}{\sigma}\right) - \operatorname{erf}\left(\frac{x-z_2}{\sigma}\right), \quad x \in [0,1], \quad \sigma = 0.001.$$

f>0 in the spill zone Ω_s with the prescribed amount of contaminant $\bar{\rho}=1$ injected per unit volume per unit time. f<0 represents the extraction/remediation of the contaminant from the aquifer where $\bar{\rho}=\rho$ is the current concentration in the groundwater. Initially, the groundwater is assumed clean, i.e., $\rho_0\equiv 0$ in the aquifer Ω . In scheme (4.7) and (4.9), $\partial_{\rho}f=0$ on [0,0.5] and $\partial_{\rho}f(x,\bar{\rho})=-\psi(x;0.9,1)$ on [0.5,1]. The observational time period T=10. The potential field $G(x,\rho_T)$ is chosen to be

(5.3)
$$G(x, \rho_T) = \rho_T^2 \psi(x; 0.9, 1)/2.$$

We first carry out numerical experiments to investigate the convergence of the time-fractional MFC approximation to the concentration ρ of the contaminant for different values of the fractional order α in comparison with the MFC constrained with the integer-order diffusive advective transport PDE. Since the analytical solution is not available, we compute the reference solution with a fine time step size $\tau_{ref} = 1/2048$ and a fine spatial mesh size $h_{ref} = 1/160$ to measure the temporal and spatial convergence rates r_t and r_s , respectively:

$$\|\rho_T(\cdot) - \rho_h(\cdot, T)\|_{L^2(\Omega)} \le Q(\tau^{r_t} + h^{r_s}).$$

The numerical results are presented in Tables 5.1 and 5.2, which indicate the temporal and spatial convergence of the approximation.

Table 5.1 The temporal convergence of the MFC approximation to ρ in section 5.1.

	$\alpha = 0.1$		$\alpha = 0.5$		$\alpha = 0.9$	
$\overline{\tau}$	$\ \rho_T - \rho_h\ $	r_t	$\ \rho_T - \rho_h\ $	r_t	$\ \rho_T - \rho_h\ $	r_t
1/32	1.08E-02		8.42 E-03		4.43E-03	
1/64	5.39E-03	1.01	4.21E-03	1.00	2.29E-03	0.95
1/128	2.61E-03	1.04	2.06E-03	1.03	1.15E-03	0.98
1/256	1.22E-04	1.09	9.66E-04	1.09	5.59E-04	1.04

Table 5.2 The spatial convergence of the MFC approximation to ρ in section 5.1.

	$\alpha = 0.1$		$\alpha = 0.5$		$\alpha = 0.9$	
h	$\ \rho_T - \rho_h\ $	r_s	$\ \rho_T - \rho_h\ $	r_s	$\ \rho_T - \rho_h\ $	r_s
1/4	4.46E-01		4.11E-01		3.85E-01	
1/8	1.75E-01	1.35	1.66E-01	1.31	1.61E-01	1.26
1/16	7.22E-02	1.28	6.61 E-02	1.33	7.14E-02	1.17
1/20	4.36E-02	2.25	4.49E-02	1.72	4.75E-02	1.82

With the numerically tested convergence of the MFC approximation, we then conduct numerical experiments to assess the performance of the MFC for different values of the fractional order α in comparison with the MFC constrained with the integer-order diffusive advective transport PDE. We use the spatial mesh size h=1/32 and the time step size $\tau=Th^2$ in the MFC simulation and present the plots of the concentration ρ , the optimal velocity $v(=-\partial_x\phi)$, and the terminal concentration ρ_T in Figure 5.1. The first row is for the Fickian diffusive advective transport with $\kappa=0$ in (2.3), and the second through fourth rows are for the subdiffusive advective transport with $\kappa=1$ and $\alpha=0.3$, 0.5, and 0.8, respectively. In all the scenarios, the MFC is observed to successfully remediate all the contaminant and to ensure the supply of clean water in the groundwater supply zone over the entire operational time period.

5.1.2. Numerical experiment 1(b). The problem setting is set to be the same as in section 5.1.1 except that the source and sink term of the contaminant leakage is modified as follows:

(5.4)
$$f(x,\bar{\rho}) = \begin{cases} \psi(x;0,0.1)\,\bar{\rho}, & (x,t) \in [0,0.5] \times [0,1], \\ -\psi(x;0.9,1)\,\rho, & (x,t) \in [0.5,1] \times [0,10], \\ 0 & \text{elsewhere.} \end{cases}$$

That is, the contaminant leakage takes place during the time period [0,1], but the objective of the MFC is to ensure that the contaminant can be eliminated in the groundwater supply zone during a much longer time period [0,10]. Since the time dependence of f on the time t is through $\bar{\rho}$, the time dependence of f can be viewed as $\rho = 1$ on [0,1] and 0 on [0,10].

Due to the similarity of the problem to the one in section 5.1.1, we only present the concentration ρ of the contaminant, the optimal velocity v, and the terminal concentration ρ_T of the contaminant of the subdiffusive advective transport PDE with $\kappa = 1$ and $\alpha = 0.5$ in (2.3) in comparison with those of the Fickian diffusive advective transport PDE with $\kappa = 0$ in (2.3). We present the plots in Figure 5.2. We observe that with the optimal velocity, the groundwater supply zone is remained contaminant free during the long time period [0,10].

5.1.3. Numerical experiment 1(c). We only modify the source and sink term in (5.1) as follows while keeping all the other parameters unchanged:

(5.5)
$$f(x,\bar{\rho}) = \begin{cases} \psi(x;0,0.5) \ \bar{\rho}, & x \in [0,0.5], \\ -\psi(x;0.5,0.9) \ \rho, & x \in [0.5,1] \end{cases}$$

with $\bar{\rho} = 1$. We present the concentration ρ of the contaminant, the optimal velocity v, and the terminal concentration ρ_T of the contaminant of the subdiffusive advective

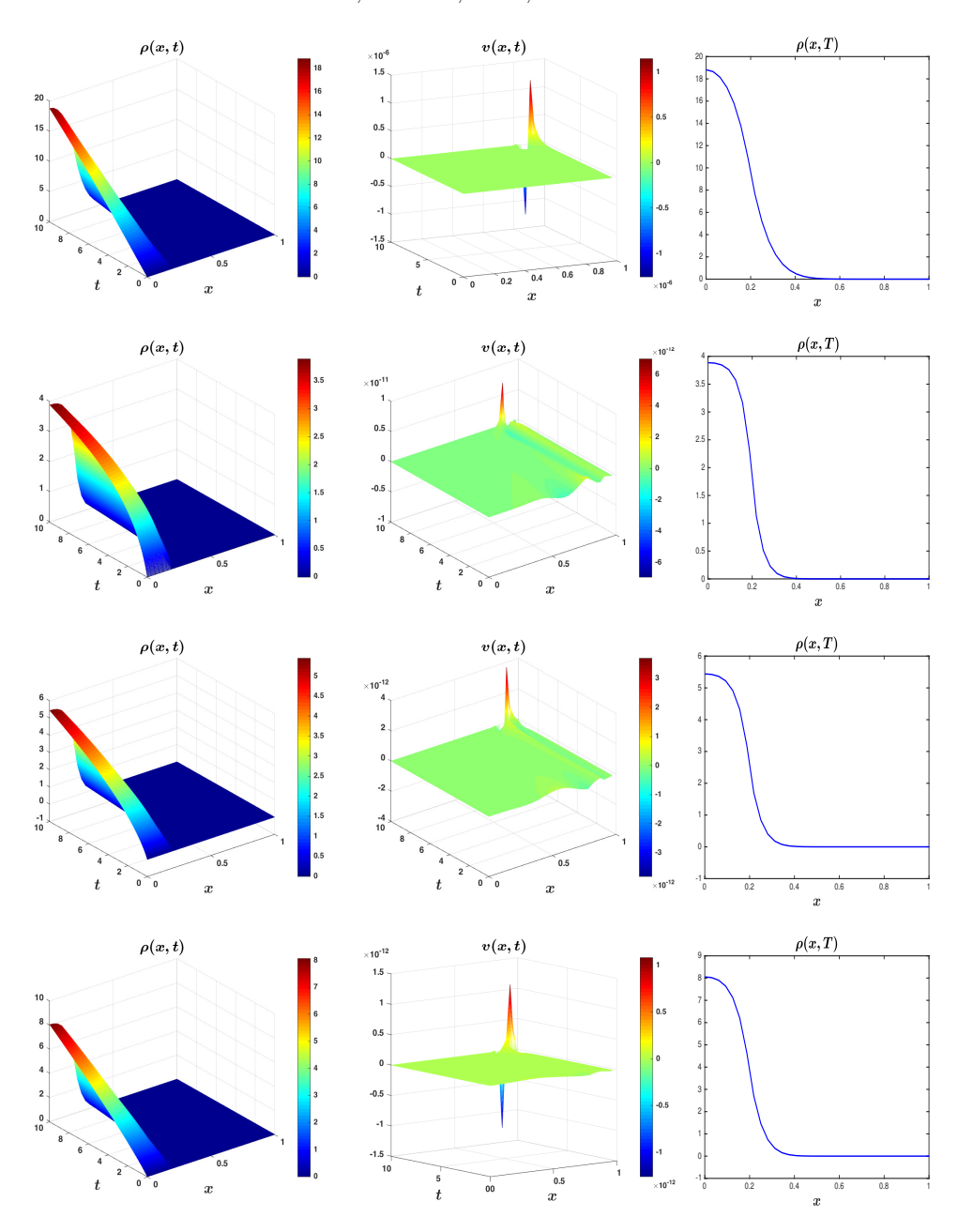


Fig. 5.1. Performance of the one-dimensional MFC in section 5.1.1 with f given in (5.1). Left column: the concentration $\rho(x,t)$; middle column: the optimal velocity v(x,t); right column: the terminal concentration $\rho_T(x,t)$. The first row: the Fickian diffusive advective transport with $\kappa=0$ in (2.3); the second through fourth rows: the subdiffusive advective transport with $\kappa=1$ and $\alpha=0.3$, 0.5, and 0.8, respectively, in (2.3).

transport PDE with $\kappa=1$ and $\alpha=0.5$ in (2.3) in comparison with those of the Fickian diffusive advective transport PDE with $\kappa=0$ in (2.3). We present the plots in Figure 5.3.

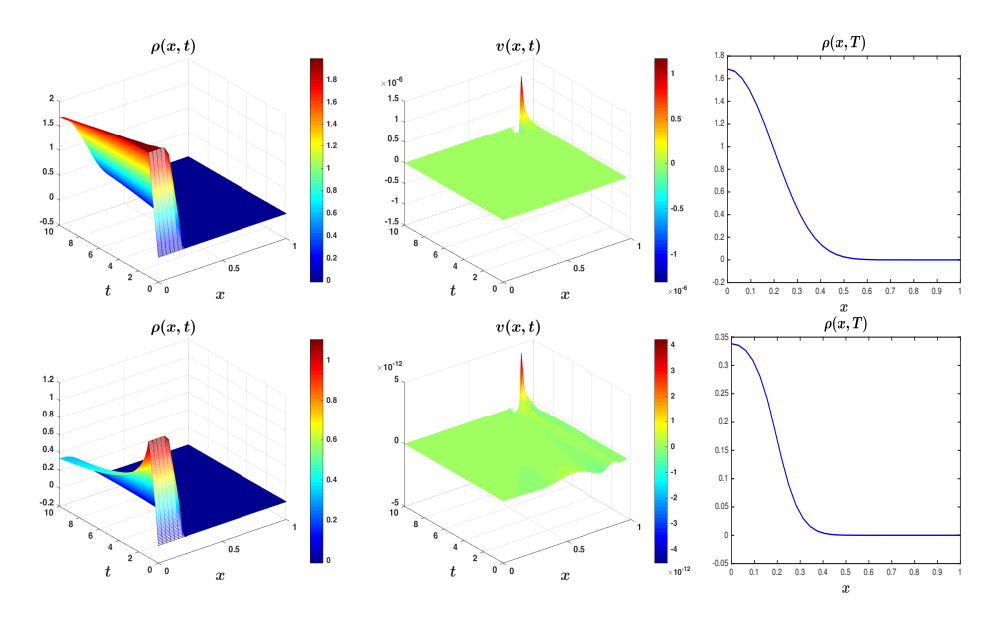


Fig. 5.2. Performance of the one-dimensional MFC in section 5.1.2 with f given in (5.4). The first row from left to right: Plots of the concentration ρ , the optimal velocity v, and the terminal concentration ρ_T of the Fickian diffusive advective transport PDE with $\kappa=0$ in (2.3). The plots in the second row correspond to those of the subdiffusive advective transport PDE with $\kappa=1$ and $\alpha=0.5$ in (2.3).

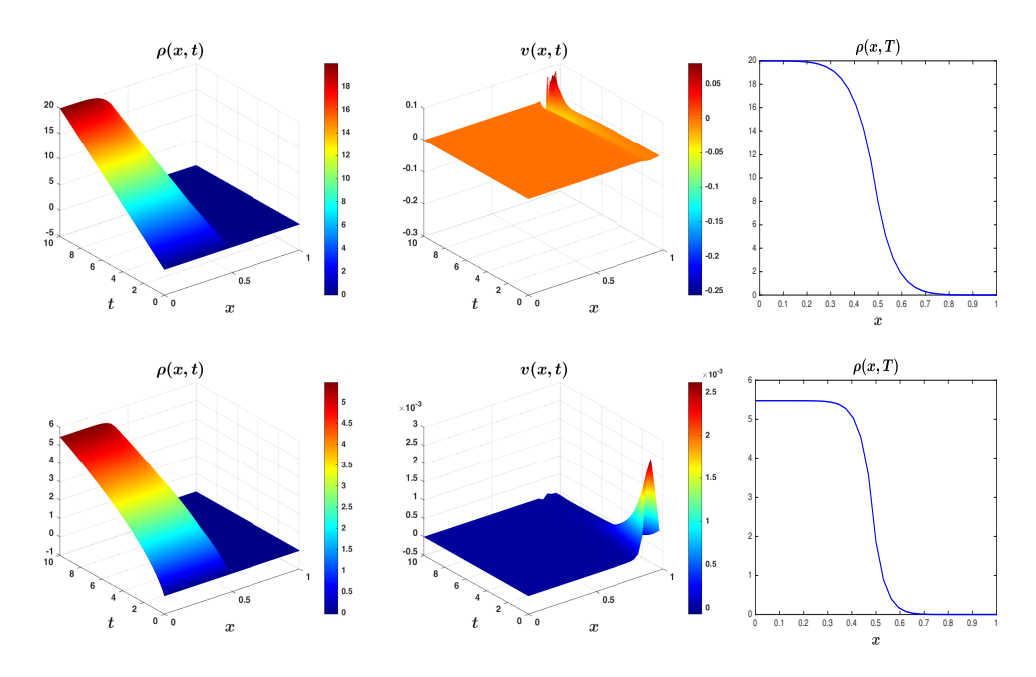


Fig. 5.3. Performance of the one-dimensional MFC in section 5.1.3 with f given in (5.5). The first row from left to right: Plots of the concentration ρ , the optimal velocity v, and the terminal concentration ρ_T of the Fickian diffusive advective transport PDE with $\kappa=0$ in (2.3). The plots in the second row correspond to those of the subdiffusive advective transport PDE with $\kappa=1$ and $\alpha=0.5$ in (2.3).

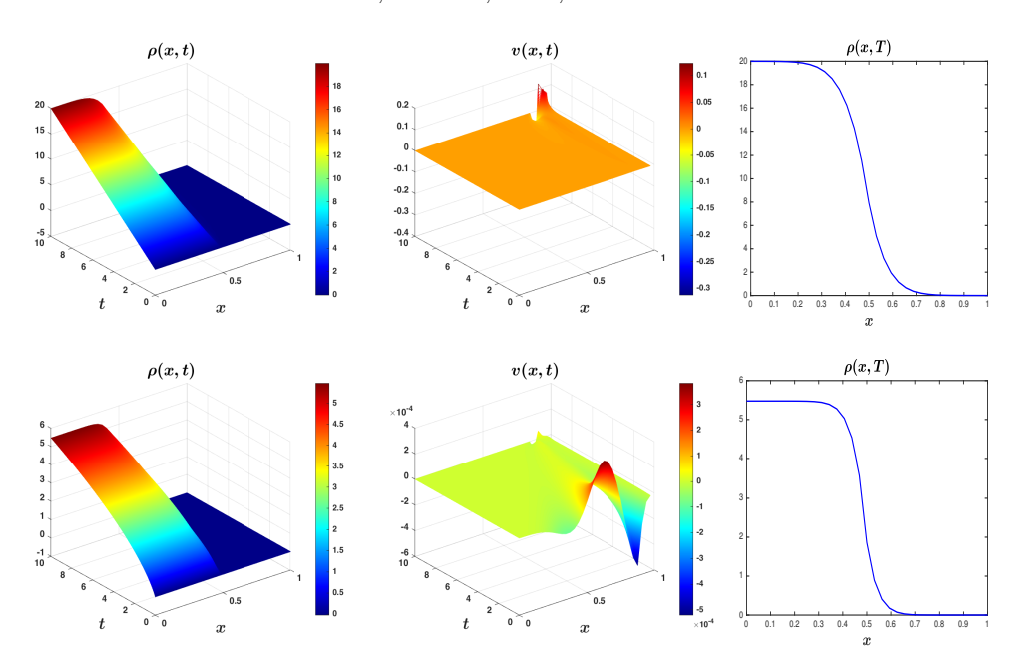


FIG. 5.4. Performance of the one-dimensional MFC in section 5.1.4 with f given in (5.6). The first row from left to right: Plots of the concentration ρ , the optimal velocity v, and the terminal concentration ρ_T of the Fickian diffusive advective transport PDE with $\kappa=0$ in (2.3). The plots in the second row correspond to those of the subdiffusive advective transport PDE with $\kappa=1$ and $\alpha=0.5$ in (2.3).

5.1.4. Numerical experiment 1(d). In this set of experiments we only modify the source and sink term in section 5.1.3 as follows while keeping all the other parameters unchanged:

(5.6)
$$f(x,\bar{\rho}) = \begin{cases} \psi(x;0,0.5) \,\bar{\rho}, & x \in [0,0.5], \\ -\psi(x;0.5,0.9) \,\rho, & x \in [0.5,1] \end{cases}$$

with $\bar{\rho} = 2$. We present the concentration ρ of the contaminant, the optimal velocity v, and the terminal concentration ρ_T of the contaminant of the subdiffusive advective transport PDE with $\kappa = 1$ and $\alpha = 0.5$ in (2.3) in comparison with those of the Fickian diffusive advective transport PDE with $\kappa = 0$ in (2.3) in Figure 5.4.

- **5.2. Performance of the two-dimensional MFC.** The problem setting is as follows: The aquifer $\Omega = (0,1)^2$, the spill zone $\Omega_s = (0,0.1)^2$, and the groundwater supply zone $\Omega_w = (0.9,1)^2$.
- **5.2.1. Numerical experiment 2(a).** The source and sink term f is an extension of (5.1) and is of the form

(5.7)
$$f(x,y,\bar{\rho}) = \begin{cases} \psi(x;0,0.1)\psi(y;0,0.1)\ \bar{\rho}, & (x,y) \in (0,0.5)^2, \\ -\psi(x;0.9,1)\psi(y;0.9,1)\ \rho, & (x,y) \in (0.5,1)^2, \\ 0 & \text{elsewhere} \end{cases}$$

with $\bar{\rho} = 1$ and $\psi(\cdot; z_1, z_2)$ given in (5.2). $G(x, y, \rho_T)$ is a two-dimensional extension of (5.3):

(5.8)
$$G(x, y, \rho_T) = \rho_T^2 \psi(x; 0.9, 1) \psi(y; 0.9, 1) / 2, \quad (x, y) \in \Omega.$$

All other parameters are chosen to be the same as in section 5.1.1. In Figure 5.5 we present the plots of $\rho_T(x,y)$, and the x component $v_x(x,y,T) (= -\partial_x \phi(x,y,T))$ and the y component $v_y(x,y,T) (= -\partial_y \phi(x,y,T))$ of the velocity field $\mathbf{v} = (v_x,v_y)$ for the Fickian diffusive advective transport and the subdiffusive advective transport with different values of the fractional order $\alpha = 0.3, 0.5$, and 0.8, respectively.

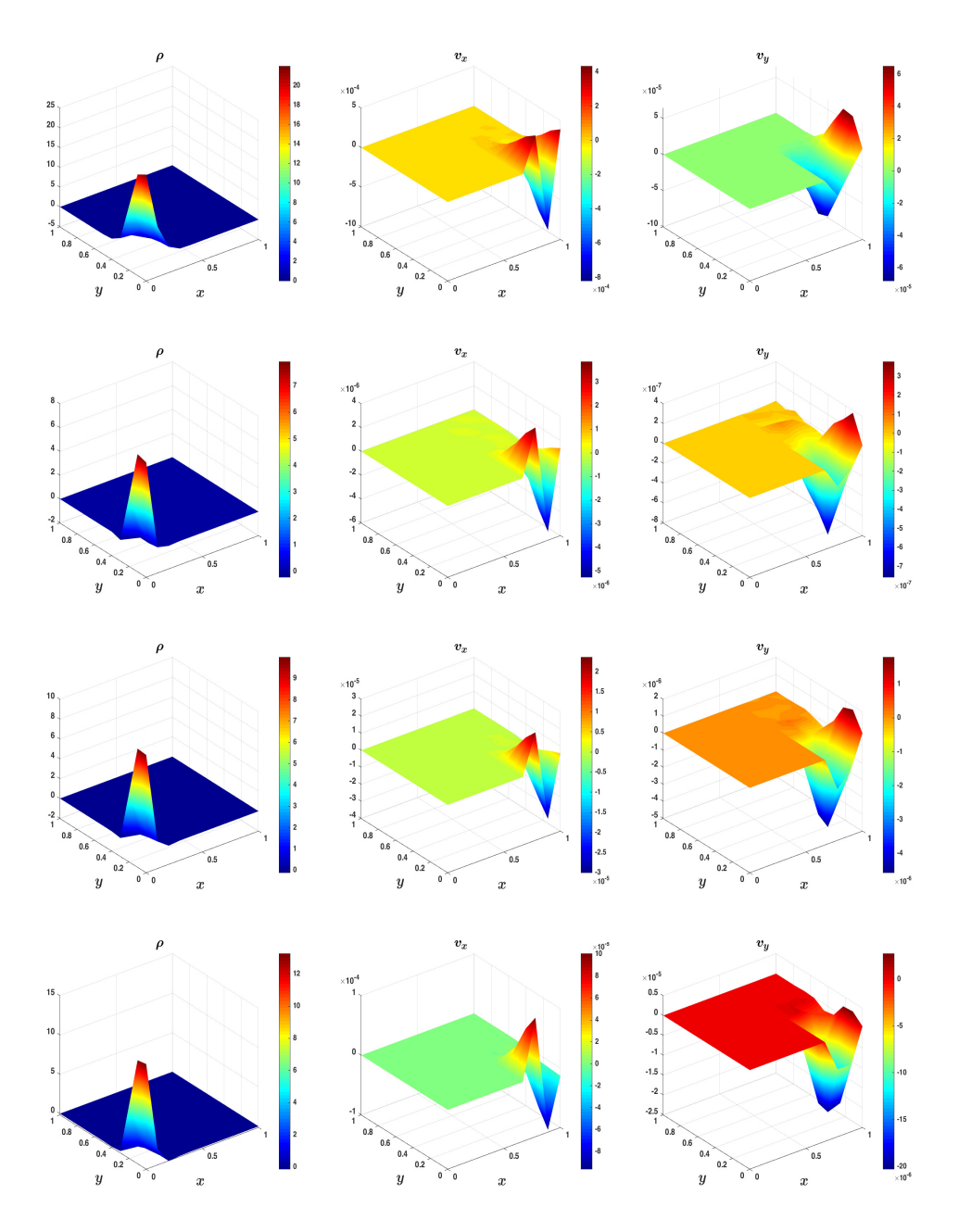


Fig. 5.5. Performance of the two-dimensional MFC in section 5.2.1 with f given in (5.7). Left column: The terminal concentration $\rho_T(x,y)$; middle (resp., right) column: the x-component $v_x(x,y,T)$ (resp., the y-component $v_y(x,y,T)$) of the optimal terminal velocity \boldsymbol{v} . The first row: The Fickian diffusive advective transport with $\kappa=0$ in (2.3); the second through fourth rows: the subdiffusive advective transport with $\kappa=1$ and $\alpha=0.3, 0.5,$ and 0.8, respectively, in (2.3).

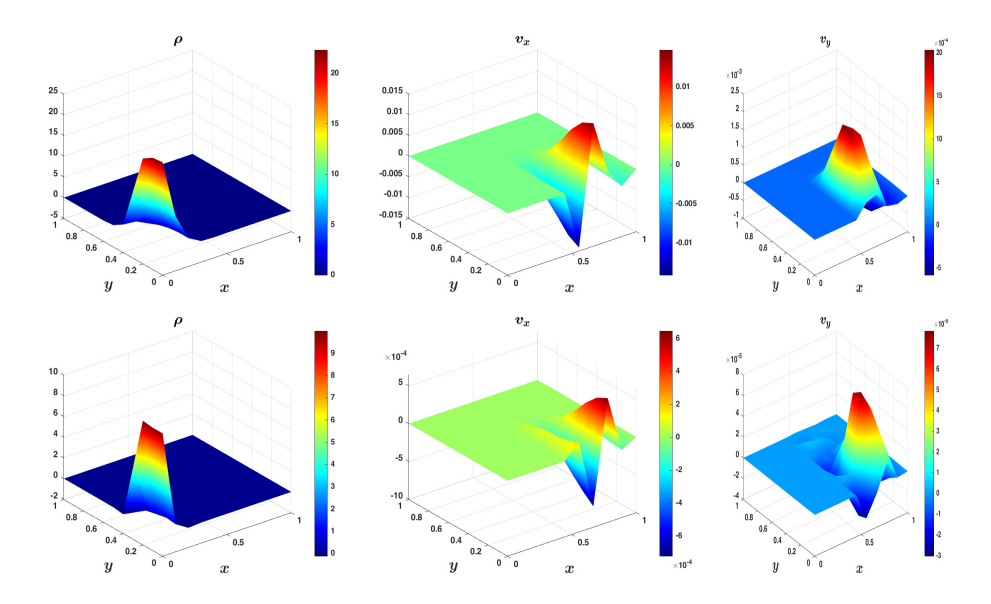


FIG. 5.6. Performance of the two-dimensional MFC in section 5.2.2 with f given in (5.9). The first row from left to right: Plots of the terminal concentration ρ_T , the x-component $v_x(x,y,T)$ of the optimal terminal velocity \mathbf{v} , and the y-component $v_y(x,y,T)$ of the terminal velocity of the Fickian diffusive advective transport PDE with $\kappa=0$ in (2.3); the plots in the second row correspond to those of the subdiffusive advective transport PDE with $\kappa=1$ and $\alpha=0.5$ in (2.3).

5.2.2. Numerical experiment **2(b)**. In this set of numerical experiments we modify the source and sink term in (5.7) as follows while keeping all the other parameters unchanged:

$$(5.9) \qquad f(x,y,\bar{\rho}) = \begin{cases} \psi(x;0,0.3)\psi(y;0,0.3)\;\bar{\rho}, & (x,y) \in (0,0.5)^2, \\ -\psi(x;0.6,0.9)\psi(y;0.6,0.9)\;\rho, & (x,y) \in (0.5,1)^2, \\ 0 & \text{elsewhere} \end{cases}$$

with $\bar{\rho} = 1$. In Figure 5.6 we present the terminal concentration ρ_T , the x-component $v_x(x, y, T)$, and the y-component $v_y(x, y, T)$ of the optimal terminal velocity \boldsymbol{v} of the subdiffusive advective transport PDE with $\kappa = 1$ and $\alpha = 0.5$ in (2.3) in comparison with those of the Fickian diffusive advective transport PDE with $\kappa = 0$ in (2.3).

5.2.3. Numerical experiment **2**(c). The problem setting is the same as in section 5.2 except that the source and sink term of the contaminant leakage is as follows:

$$(5.10) \quad f(x,y,\bar{\rho}) = \left\{ \begin{array}{ll} \psi(x;0,0.3)\psi(y;0,0.3)\;\bar{\rho}, & (x,y,t) \in (0,0.5)^2 \times [0,1], \\ -\psi(x;0.6,0.9)\psi(y;0.6,0.9)\;\rho, & (x,y,t) \in (0.5,1)^2 \times [0,10], \\ 0 & \text{elsewhere} \end{array} \right.$$

with $\bar{\rho} = 1$. In Figure 5.7 we present the terminal concentration ρ_T , the x-component $v_x(x,y,T)$, and the y-component $v_y(x,y,T)$ of the optimal terminal velocity \boldsymbol{v} of the subdiffusive advective transport PDE with $\kappa = 1$ and $\alpha = 0.5$ in (2.3) in comparison with those of the Fickian diffusive advective transport PDE with $\kappa = 0$ in (2.3).

In summary, in this section we carry out one- and two-dimensional numerical experiments to investigate the performance of the time-fractional MFC, which show

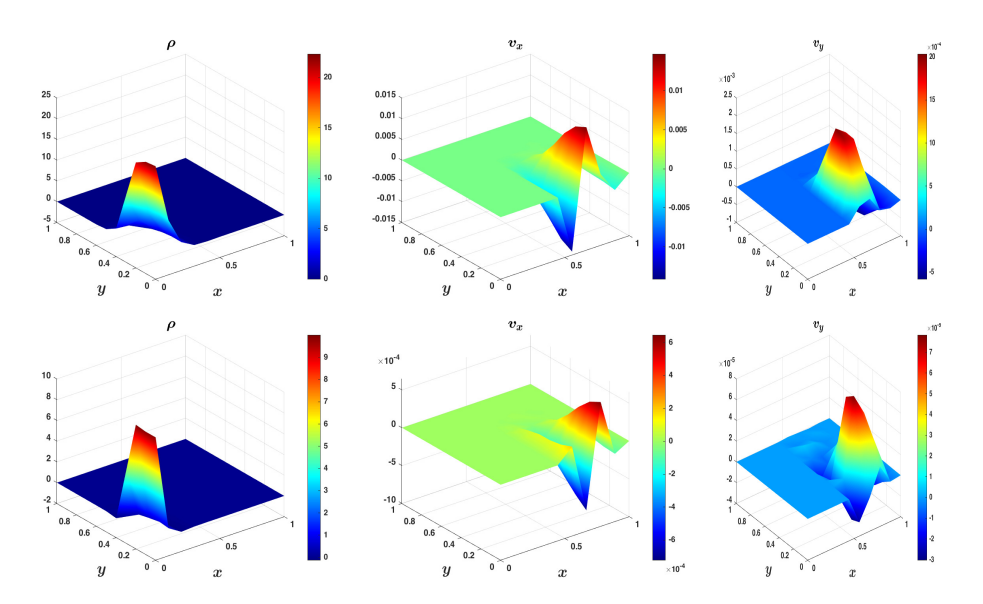


FIG. 5.7. Performance of the two-dimensional MFC in section 5.2.3 with f given in (5.10). The first row from left to right: Plots of the terminal concentration ρ_T , the x-component $v_x(x,y,T)$ of the optimal terminal velocity \mathbf{v} , and the y-component $v_y(x,y,T)$ of the terminal velocity of the Fickian diffusive advective transport PDE with $\kappa=0$ in (2.3); the plots in the second row correspond to those of the subdiffusive advective transport PDE with $\kappa=1$ and $\alpha=0.5$ in (2.3).

that the MFC can optimize and remediate the transport of the contaminant to ensure the safe supply of the groundwater to the public during the entire time period of the spill and beyond for different scenarios. Furthermore, these experiments suggest that the time-fractional MFC formulation does not seem to be sensitive to the variation of the parameters in the optimization problem.

6. Concluding remarks. In this paper we develop a multiple time-scale time-fractional MFC to model the accidental spill of a hazardous contaminant, which is a representative and recurrent environmental threat to the public. We use the first-order optimality condition to the MFC and introduce a Lagrangian multiplier to reformulate the optimization problem to a strongly coupled nonlinear time-fractional system (3.8) that consists of a multiple time-scale time-fractional subdiffusive advective transport PDE in terms of the concentration ρ of the contaminant and a backward multiple time-scale time-fractional Hamilton–Jacobi PDE in terms of the pseudopotential ϕ , which gives the optimal velocity field v that governs the transport of the contaminant. We derive a sequentially decoupled time-stepping finite element method (4.7) and (4.9) for the numerical simulation of the system. We then carry out numerical experiments to investigate the performance of the MFC. Preliminary test runs indicate that the MFC can transport and remediate the contaminant to ensure the safe supply of the groundwater to the public during the entire time period of the spill and beyond.

Although the results in this paper indicate strong potential of the MFC in subsurface flow and transport applications, significant effort and further study on the MFC are required for realistic applications, such as groundwater contaminant transport and remediation [4, 24], CO₂ sequestration [40], and hydrocarbon recovery [3, 22]. We briefly outline possible future directions we may pursue:

- (i) In this paper we developed the MFC (2.1) and (2.3) for the simplest spill scenario, which takes place in the fully saturated zone below the water table and the contaminant is fully miscible with the groundwater [4]. In reality the velocity \boldsymbol{v} in the transport PDE (2.3) may be constrained both by the Darcy's law with the proportionality parameter given by the intrinsic permeability of the geological formation and by the mass conservation of the fluid mixture [4]. In the closely related enhanced hydrocarbon recovery, the proportionality parameter may also be inversely proportional to the ρ -dependent viscosity of the fluid mixture [3, 22, 52].
 - In a slanted two-dimensional or full three-dimensional aquifer, the Darcy's law will be augmented by an additional term accounting for the contribution of the gravitational influence. One of the future directions is to develop an MFC that fully takes into account this information.
- (ii) If the contaminant happens to be a nonaqueous phase liquid (NAPL) that is immiscible with the groundwater, then the balance PDE will be formulated for each of the water and NAPL phases with strongly nonlinear and degenerate relative permeability and Buckley-Leverett type of S-shaped fractional flow functions [24, 31]. A similar scenario happens if the spill takes place in the unsaturated zone above the water table or in secondary hydrocarbon recovery [3, 22, 24, 31, 40].
 - In realistic three space dimensions, the influence of gravity could significantly alter the shape of the fractional flow function and further complicate the flow pattern.
- (iii) If the spill involves multiple components with significantly different molecular weights, then the mass of each phase or of each component in each phase is not conserved. Instead, the total mass of each component in all the phases is conserved, and in particular phase change could happen as the temperature or pressure changes. The same scenario also happens in hydrocarbon recovery process [3, 24, 54].
 - Both multiphase and multiphase multicomponent models in (ii) and (iii) will significantly complicate the MFC framework, which is not so clear at this moment and requires significant effort to investigate.
- (iv) Subsurface geological formation is often highly heterogeneous. Its information is usually available only near the injection and production (or monitoring) wells and so is very limited. Consequently, this often introduces significant noise and uncertainty to the models outlined above and further complicates the problems [2, 17, 53, 57, 60, 63].
- (v) Fractional PDEs have been widely used in different applications including anomalously diffusive transport in subsurface porous media (e.g., [1, 18, 20, 42, 56, 58, 59]). In this paper, we extend the works to develop a time-fractional MFC to model accidental spill of hazardous contaminant in subsurface porous medium and its remediation to ensure a safe water supply to the public.
 - It remains to conduct rigorous mathematical analysis on the well-posedness and regularity of the MFC and the corresponding numerical analysis of the numerical method, which could in turn ensure the convergence of the Newton's method in the optimization of the problems. These issues could be investigated, e.g., via the analytical approach in [7, 14, 15, 50].

Acknowledgment. The authors would like to express their sincere thanks to the referees for their very helpful comments and suggestions, which greatly improved the quality of this paper.

REFERENCES

- H. Antil, E. Otárola, and A. J. Salgado, A space-time fractional optimal control problem: Analysis and discretization, SIAM J. Control Optim., 54 (2016), pp. 1295–1328, https://doi.org/10.1137/15M1014991.
- [2] I. Babuška, R. Tempone, and G. E. Zouraris, Galerkin finite element approximations of stochastic elliptic differential equations, SIAM J. Numer. Anal., 42 (2004), pp. 800–825, https://doi.org/10.1137/S0036142902418680.
- [3] M. Balhoff, An Introduction to Multiphase, Multicomponent Reservoir Simulation, Developments in Petroleum Science 75, Elsevier, 2022.
- [4] J. Bear, Dynamics of Fluids in Porous Media, Elsevier, New York, 1972.
- [5] D. Benson, R. Schumer, M. Meerschaert, and S. Wheatcraft, Fractional dispersion, Lévy motions, and the MADE tracer tests, Transp. Porous Media, 42 (2001), pp. 211–240.
- [6] F. Brezzi and M. Fortin, Mixed and Hybrid Finite Element Methods, Springer Ser. Comput. Math. 15, Springer-Verlag, New York, 1991.
- [7] F. CAMILLI AND R. DE MAIO, A time-fractional mean field game, Adv. Differential Equations, 24 (2019), pp. 531–554.
- [8] F. CAMILLI AND S. DUISEMBAY, Approximation of Hamilton-Jacobi equations with the Caputo time-fractional derivative, Minimax Theory Appl., 5 (2020), pp. 199–220.
- [9] F. CAMILLI, S. DUISEMBAY, AND Q. TANG, Approximation of an optimal control problem for the time-fractional Fokker-Planck equation, J. Dyn. Games, 8 (2021), pp. 381–402.
- [10] F. CAMILI AND A. GOFFI, Existence and regularity results for viscous Hamilton-Jacobi equations with Caputo time-fractional derivative, NoDEA Nonlinear Differential Equations Appl., 27 (2020), 22.
- [11] L. CAO AND R. HE, Gas diffusion in fractal porous media, Combust. Sci. Technol., 182 (2010), pp. 822–841.
- [12] R. CARMONA AND M. LAURIÈRE, Convergence analysis of machine learning algorithms for the numerical solution of mean field control and games I: The ergodic case, SIAM J. Numer. Anal., 59 (2021), pp. 1455–1485, https://doi.org/10.1137/19M1274377.
- [13] A. CHAMBOLLE AND T. POCK, A first-order primal-dual algorithm for convex problems with applications to imaging, J. Math. Imaging Vision, 40 (2011), pp. 120–145.
- [14] O. CHEPIZHKO AND F. PERUANI, Diffusion, subdiffusion, and trapping of active particles in heterogeneous media, Phys. Rev. Lett., 111 (2013), pp. 1-5.
- [15] I. CHOWDHURY, O. ERSLAND, AND E. R. JAKOBSEN, On numerical approximations of fractional and nonlocal mean field games, Found. Comput. Math., 23 (2023), pp. 1381–1431, https://doi.org/10.1007/s10208-022-09572-w.
- [16] M. CIRANT AND A. GOFFI, On the existence and uniqueness of solutions to timedependent and fractional MFG, SIAM J. Math. Anal., 51 (2019), pp. 913–954, https://doi.org/10.1137/18M1216420.
- [17] G. DAGAN, Flow and Transport in Porous Formations, Springer, New York, 1989.
- [18] Z. DENG, J. DE LIMA, M. DE LIMA, AND V. SINGH, A fractional dispersion model for overland solute transport, Water Resour. Res., 42 (2006), W03416.
- [19] M. Dentz, A. Cortis, H. Scher, and B. Berkowitz, Time behavior of solute transport in heterogeneous media: Transition from anomalous to normal transport, Adv. Water Resour., 27 (2004), pp. 155–173.
- [20] M. D'ELIA, Q. Du, C. Glusa, M. Gunzburger, X. Tian, and Z. Zhou, Numerical methods for nonlocal and fractional models, Acta Numer., 29 (2020), pp. 1–124.
- [21] L. EVANS, Partial Differential Equations, 2nd ed., Grad. Stud. Math. 19, American Mathematical Society, Providence, RI, 2010.
- [22] R. E. EWING, ED., The Mathematics of Reservoir Simulation, Frontiers Appl. Math. 1, SIAM, Philadelphia, 1983, https://doi.org/10.1137/1.9781611971071.
- [23] D. A. GOMES AND E. PIMENTEL, Time-dependent mean-field games with logarithmic nonlinearities, SIAM J. Math. Anal., 47 (2015), pp. 3798–3812, https://doi.org/10.1137/140984622.
- [24] R. HELMIG, Multiphase Flow and Transport Processes in the Subsurface, Springer-Verlag, Berlin, 1997.

- [25] M. Huang, R. P. Malhamé, and P. E. Caines, Large population stochastic dynamic games: Closed-loop McKean-Vlasov systems and the Nash certainty equivalence principle, Commun. Inf. Syst., 6 (2006), pp. 221–252.
- [26] Y. KANG, S. LIU, H. ZHANG, W. LI, Z. HAN, S. OSHER, AND V. POOR, Joint sensing task assignment and collision-free trajectory optimization for mobile vehicle networks using mean-field games, IEEE Internet Things J., 8 (2021), pp. 8488–8503.
- [27] Z. KOBEISSI, On classical solutions to the mean field game system of controls, Comm. Partial. Differential Equations, 51 (2019), pp. 913–954.
- [28] A. KRÖNER, K. KUNISCH, AND B. VEXLER, Semismooth Newton methods for optimal control of the wave equation with control constraints, SIAM J. Control Optim., 49 (2011), pp. 830–858, https://doi.org/10.1137/090766541.
- [29] J.-M. LASRY AND P.-L. LIONS, Mean field games, Jpn. J. Math., 2 (2007), pp. 229-260.
- [30] W. Lee, S. Liu, H. Tembine, W. Li, and S. Osher, Controlling propagation of epidemics via mean-field control, SIAM J. Appl. Math., 81 (2021), pp. 190–207, https://doi.org/10.1137/20M1342690.
- [31] R. LEVEQUE, Finite Volume Methods for Hyperbolic Problems, Cambridge Texts Appl. Math., Cambridge University Press, Cambridge, 2002.
- [32] W. Li, W. Lee, and S. Osher, Computational mean-field information dynamics associated with reaction-diffusion equations, J. Comput. Phys., 466 (2022), 111409.
- [33] A. Lin, S. Fung, W. Li, L. Nurbekyan, and S. Osher, Alternating the population and control neural networks to solve high-dimensional stochastic mean field games, Proc. Natl. Acad. Sci. USA, 118 (2021), e2024713118.
- [34] Y. LIN AND C. Xu, Finite difference/spectral approximations for the time-fractional diffusion equation, J. Comput. Phys., 225 (2007), pp. 1552–1553.
- [35] F. LIU, S. SHEN, V. ANH, AND I. TURNER, Analysis of a discrete non-Markovian random walk approximation for the time fractional diffusion equation, ANZIAM, 46 (2004/05), pp. C488-C504.
- [36] S. LIU, M. JACOBS, W. LI, L. NURBEKYAN, AND S. J. OSHER, Computational methods for first-order nonlocal mean field games with applications, SIAM J. Numer. Anal., 59 (2021), pp. 2639–2668, https://doi.org/10.1137/20M1334668.
- [37] M. MEERSCHAERT AND A. SIKORSKII, Stochastic Models for Fractional Calculus, De Gruyter Stud. Math. 43, Walter de Gruyter, Berlin, 2012.
- [38] R. METZLER AND J. KLAFTER, The random walk's guide to anomalous diffusion: A fractional dynamics approach, Phys. Rep., 339 (2000).
- [39] J. Moore, J. Palmer, Y. Liu, T. Roussel, J. Brennan, and K. Gubbins, Adsorption and diffusion of argon confined in ordered and disordered microporous carbons, Appl. Surf. Sci., 256 (2010), pp. 5131–5136.
- [40] J. NORDBOTTEN AND M. CELIA, Geological Storage of CO₂: Modeling Approaches for Large-Scale Simulation, Wiley, Hoboken, NJ, 2012.
- [41] H. Nosratipour, F. Sarani, O. Fard, and A. Borzabadi, An adaptive nonmonotone truncated Newton method for optimal control of a class of parabolic distributed parameter systems, Engrg. Comput., 36 (2020), pp. 689–702.
- [42] R. PAULOO, G. FOGG, Z. GUO, AND C. HENRI, Mean flow direction modulates non-Fickian transport in a heterogeneous alluvial aquifer-aquitard system, Water Resour. Res., 57 (2021), e2020WR028655.
- [43] I. Podlubny, Fractional Differential Equations, Academic Press, 1999.
- [44] L. RUTHOTTO, S. OSHER, W. LI, L. NURBEKYAN, AND S. FUNG, A machine learning framework for solving high-dimensional mean field game and mean field control problems, Proc. Natl. Acad. Sci. USA, 117 (2020), pp. 9183–9193.
- [45] K. Sakamoto and M. Yamamoto, Initial value/boundary value problems for fractional diffusion-wave equations and applications to some inverse problems, J. Math. Anal. Appl., 382 (2011), pp. 426–447.
- [46] R. SCHUMER, D. BENSON, M. MEERSCHAERT, AND B. BAEUMER, Fractal mobile/immobile solute transport, Water Resour. Res., 39 (2003), 1296.
- [47] R. SCHUMER, D. BENSON, M. MEERSCHAERT, AND S. WHEATCRAFT, Eulerian derivation of the fractional advection-dispersion equation, J. Contam. Hydrol., 48 (2001), pp. 69–88.
- [48] M. STYNES, E. O'RIORDAN, AND J. L. GRACIA, Error analysis of a finite difference method on graded meshes for a time-fractional diffusion equation, SIAM J. Numer. Anal., 55 (2017), pp. 1057–1079, https://doi.org/10.1137/16M1082329.
- [49] Z. Sun and X. Wu, A fully discrete difference scheme for a diffusion-wave system, Appl. Numer. Math., 56 (2006), pp. 193–209.

- [50] Q. TANG AND F. CAMILLI, Variational time-fractional mean field games, Dyn. Games Appl., 10 (2020), pp. 573–588.
- [51] F. TRÖLTZSCH, On the Lagrange-Newton-SQP method for the optimal control of semilinear parabolic equations, SIAM J. Control Optim., 38 (1999), pp. 294–312, https://doi.org/10.1137/S0363012998341423.
- [52] H. WANG, D. LIANG, R. E. EWING, S. L. LYONS, AND G. QIN, An approximation to miscible fluid flows in porous media with point sources and sinks by an Eulerian-Lagrangian localized adjoint method and mixed finite element methods, SIAM J. Sci. Comput., 22 (2000), pp. 561–581, https://doi.org/10.1137/S1064827598349215.
- [53] H. WANG, Y. REN, J. JIA, AND M. CELIA, A probabilistic collocation Eulerian-Lagrangian localized adjoint method on sparse grids for assessing CO₂ leakage through wells in randomly heterogeneous porous media, Comput. Methods Appl. Mech. Engrg., 292 (2015), pp. 35-53.
- [54] H. WANG, W. ZHAO, M. S. ESPEDAL, AND A. S. TELYAKOVSKIY, A component-based Eulerian-Lagrangian formulation for multicomponent multiphase compositional flow and transport in porous media, SIAM J. Sci. Comput., 35 (2013), pp. B462-B486, https://doi.org/10.1137/120885681.
- [55] Y. WANG AND W. LI, Accelerated information gradient flow, J. Sci. Comput., 90 (2022), 11.
- [56] Y. XIA, Y. ZHANG, C. GREEN, AND G. FOGG, Time-fractional flow equations (t-FFEs) to upscale transient groundwater flow characterized by temporally non-Darcian flow due to medium heterogeneity, Water Resour. Res., 57 (2021), e2020WR029554.
- [57] D. XIU AND G. KARNIADAKIS, Modeling uncertainty in flow simulations via generalized polynomial chaos, J. Comput. Phys., 187 (2003), pp. 137–167.
- [58] Y. Yu, P. Perdikaris, and G. Karniadakis, Fractional modeling of viscoelasticity in 3D cerebral arteries and aneurysms, J. Comput. Phys., 323 (2016), pp. 219–242.
- [59] F. ZENG, Z. ZHANG, AND G. KARNIADAKIS, Second-order numerical methods for multi-term fractional differential equations: Smooth and non-smooth solutions, Comput. Methods Appl. Mech. Engrg., 327 (2017), pp. 478–502.
- [60] D. ZHANG, Stochastic Methods for Flow in Porous Media, Coping with Uncertainties, Academic Press, New York, 2002.
- [61] Y. ZHANG, C. GREEN, AND B. BAEUMER, Linking aquifer spatial properties and non-Fickian transport in mobile-immobile like alluvial settings, J. Hydrology, 512 (2014), pp. 315–331.
- [62] X. Zheng and H. Wang, Optimal-order error estimates of finite element approximations to variable-order time-fractional diffusion equations without regularity assumptions of the solutions, IMA J. Numer. Anal., 41 (2021), pp. 1522–1545.
- [63] X. ZHENG AND H. WANG, An error estimate of a modified method of characteristics modeling advective-diffusive transport in randomly heterogeneous porous media, CSIAM Trans. Appl. Math., 3 (2022), pp. 172–190.
- [64] A. ZHOKH AND P. STRIZHAK, Non-Fickian diffusion of methanol in mesoporous media: Geometrical restrictions or adsorption-induced?, J. Chem. Phys., 146 (2017), 124704.